Published in final edited form as:
J Neurosci. 2013 February 6; 33(6): 2697–2708. doi:10.1523/JNEUROSCI.4759-12.2013.

Inositol 1,4,5-Triphosphate Drives Glutamatergic and Cholinergic Inhibition Selectively in Spiny Projection Neurons in the Striatum

Michael A. Clements, **Immani Swapna**, and **Hitoshi Morikawa**
Waggoner Center for Alcohol and Addiction Research, Section of Neurobiology, University of Texas, Austin, Austin, Texas 78712

Abstract

The striatum is critically involved in the selection of appropriate actions in a constantly changing environment. The spiking activity of striatal spiny projection neurons (SPNs), driven by extrinsic glutamatergic inputs, is shaped by local GABAergic and cholinergic networks. For example, it is well established that different types of GABAergic interneurons, activated by extrinsic glutamatergic and local cholinergic inputs, mediate powerful feedforward inhibition of SPN activity. In this study, using mouse striatal slices, we show that glutamatergic and cholinergic inputs exert direct inhibitory regulation of SPN activity via activation of metabotropic glutamate receptors (mGluRs) and muscarinic acetylcholine receptors. While pressure ejection of the group I mGluR (mGluR1/5) agonist DHPG [(*S*)-3,5-dihydroxyphenylglycine] equally engages both mGluR1 and mGluR5 subtypes, the mGluR-dependent component of IPSCs elicited by intrastriatal electrical stimulation is almost exclusively mediated by the mGluR1 subtype. Ca^{2+} release from intracellular stores specifically through inositol 1,4,5-triphospahte receptors (IP_3Rs) and not ryanodine receptors (RyRs) mediates this form of inhibition by gating two types of Ca^{2+}-activated K^+ channels (i.e., small-conductance SK channels and large-conductance BK channels). Conversely, spike-evoked Ca^{2+} influx triggers Ca^{2+} release solely through RyRs to generate SK-dependent slow afterhyperpolarizations, demonstrating functional segregation of IP_3Rs and RyRs. Finally, IP_3-induced Ca^{2+} release is uniquely observed in SPNs and not in different types of interneurons in the striatum. These results demonstrate that IP_3-mediated activation of SK and BK channels provides a robust mechanism for glutamatergic and cholinergic inputs to selectively suppress striatal output neuron activity.

Introduction

The output from the striatum to downstream basal ganglia structures plays a critical role in the selection and planning of actions (Graybiel et al., 1994). Medium-sized, GABAergic spiny projection neurons (SPNs), which constitute ~95% of striatal neurons, provide the sole output of the striatum. *In vivo* intracellular recordings have revealed that membrane potential of SPNs shifts from a quiescent hyperpolarized DOWN state (approximately −70 to −90 mV) to a depolarized UP state (approximately −50 to −60 mV), during which action potential (AP) firing occurs (Wilson and Kawaguchi, 1996; Stern et al., 1998). Coordinated excitatory inputs mainly from the cerebral cortex drive the transition to the UP state, which

Correspondence should be addressed to Hitoshi Morikawa, Section of Neurobiology, University of Texas, Austin, 2400 Speedway, PAT 402, Austin, TX 78712. morikawa@utexas.edu.

Author contributions: M.A.C., I.S., and H.M. designed research; M.A.C. and I.S. performed research; M.A.C., I.S., and H.M. analyzed data; M.A.C., I.S., and H.M. wrote the paper.

lasts for hundreds of milliseconds to seconds before switching back to the DOWN state. During the UP state, the balance between depolarizing cortical and thalamic inputs and hyperpolarizing voltage-gated K^+ conductances, together with inputs from local GABAergic and cholinergic networks, are thought to determine whether and when SPNs fire APs (Surmeier et al., 2007; Tepper et al., 2008). Single-unit recordings in behaving animals have shown that SPNs differentially exhibit increases and decreases, or pauses, in firing before and during performance of actions (Hikosaka et al., 1989; Jin and Costa, 2010; Krause et al., 2010). However, the underlying mechanisms of the pauses and whether they can occur in the UP state or represent transitions to the DOWN state remain unclear.

SPN firing is also shaped by two types of Ca^{2+}-activated K^+ channels, small-conductance SK channels and large-conductance BK channels (Pineda et al., 1992; Hopf et al., 2010). Ca^{2+} influx through voltage-gated Ca^{2+} channels (VGCCs) triggered by each AP activates these channels, thereby generating afterhyperpolarizations (AHPs) that control AP duration and interspike intervals. AP-evoked Ca^{2+} transients can be further amplified by a process called Ca^{2+} -induced Ca^{2+} release (CICR) via two types of Ca^{2+} -sensitive receptors [i.e., inositol 1,4,5-trisphosphate receptors (IP_3Rs) and ryanodine receptors (RyRs)] located on intracellular Ca^{2+} stores (Berridge, 1998). Furthermore, neurotransmitter inputs coupled to G-protein-dependent generation of second messengers elicit IP_3R- and/or RyR-dependent Ca^{2+} release to activate SK and BK channels in a variety of neurons in the CNS (Fiorillo and Williams, 2000; Morikawa et al., 2003; Gulledge and Stuart, 2005; Canepari and Ogden, 2006; Hagenston et al., 2008; Power and Sah, 2008; El-Hassar et al., 2011). Although group I metabotropic glutamate receptors (mGluRs) (mGluR1/5) and the M_1-subtype of muscarinic acetylcholine receptors (mAChRs), which are coupled to the phospholipase C (PLC)–IP_3 cascade, are expressed in virtually all SPNs (Yan et al., 2001; Gubellini et al., 2004), the role of Ca^{2+} store-dependent activation of SK and BK channels in regulating SPN activity has yet to be determined.

In this study, using mouse striatal slices, we show that the mGluR/mAChR → IP_3R → SK/BK channel pathway produces powerful suppression of depolarization-evoked SPN firing, while the AP →RyR →SK channel pathway dominates the slow component of AHPs. Furthermore, our data showing the absence of IP_3-induced Ca^{2+} release in striatal interneurons imply that IP_3 signaling plays a privileged role in glutamatergic and cholinergic input-dependent inhibitory regulation of striatal output neurons.

Materials and Methods

Animals

Male C57BL/6J mice (3–4 weeks of age) were obtained from The Jackson Laboratory and were housed under a 12 h light/dark cycle. Food and water were available *ad libitum*. All animal procedures were approved by the University of Texas Institutional Animal Care and Use Committee.

Electrophysiology

Mice were killed by cervical dislocation under isoflurane anesthesia, and oblique horizontal slices (~20–30°, 200–250 μm) containing the dorsal striatum were cut in an ice-cold solution containing the following (in mM): 205 sucrose, 2.5 KCl, 1.25 NaH_2PO_4, 7.5 $MgCl_2$, 0.5 $CaCl_2$, 10 glucose, and 25 $NaHCO_3$, saturated with 95% O_2 and 5% CO_2 (~300 mOsm/kg) and incubated >1 h at 35°C in a solution containing the following (in mM): 126 NaCl, 2.5 KCl, 1.2 NaH_2PO_4, 1.2 $MgCl_2$, 2.4 $CaCl_2$, 11 glucose, and 25 $NaHCO_3$, saturated with 95% O_2 and 5% CO_2, pH 7.4, ~295 mOsm/kg. Recordings were made at 34–35°C in the same solution perfused at ~2.5 ml/min.

Cells were visualized using an upright microscope (Olympus) with infrared/oblique illumination optics. Whole-cell recordings were made with borosilicate glass pipettes (2.2–2.8 MΩ) filled with internal solution containing the following (in mM): 115 K-gluconate, 20 KCl, 1.5 $MgCl_2$, 10 HEPES, 0.025 EGTA, 2 Mg-ATP, 0.2 Na_2-GTP, and 10 Na_2-phosphocreatine, pH 7.2, ~285 mOsm/kg, unless indicated otherwise. Series resistance was continuously monitored but left uncompensated during voltage-clamp recording experiments. Recordings were discarded if the series resistance increased beyond 20 MΩ. Bridge balance was adjusted periodically (approximately every 2–3 min) during current-clamp recording experiments. The membrane potential was corrected for a liquid junction potential of −7 mV. A Multiclamp 700B amplifier (Molecular Devices) and AxoGraph X software (AxoGraph Scientific) were used to record and collect data (filtered at 0.5–2 kHz and digitized at 1–5 kHz for voltage-clamp recordings; filtered at 10 kHz and digitized at 20 kHz for current-clamp recordings). The majority of experiments were performed in the presence of picrotoxin (100 μM) to block $GABA_A$ inputs.

For pressure ejection, patch pipettes (~2 μm tip diameter) were filled with (*S*)-3,5-dihydroxyphenylglycine (DHPG) (100 μM) or muscarine chloride (100 μM), and pressure of 20 psi was applied using a TooheySpritzer Pressure System IIe to eject the drug. Synaptic responses were evoked with a bipolar tungsten electrode in the presence of DNQX (20 μM) and picrotoxin (100 μM) to block AMPA and $GABA_A$ receptors and slices were preincubated with MK-801 (10 μM) to block NMDA receptors.

Flash photolysis

Cells were dialyzed with caged IP_3 (400 μM) through the whole-cell pipette for 15–20 min after break-in. A brief UV flash (~1 ms) was applied with a xenon arc lamp driven by a photolysis system (Cairn Research) to rapidly photolyze caged IP_3 (~3 ms) (Walker et al., 1989). The UV flash was focused through a 60× objective onto a 350 μm area surrounding the recorded cell. The Cairn system has the capacity to vary the intensity of UV flash, which was measured at the tip of the objective (expressed in microjoules). The degree of photolysis of caged compounds is known to be proportional to the UV flash intensity (McCray et al., 1980). The maximal UV flash intensity was ~180–250 μJ with our system, depending on the age of the xenon arc lamp at the time of experiments.

Ca^{2+} imaging

Fluorescence imaging of $[Ca^{2+}]_i$ was mostly done using Fluo-4FF (Invitrogen) as Ca^{2+} indicators. Some of the imaging experiments were performed with Fluo-4 or Fluo-5F. These Ca^{2+} indicators were loaded into the cell via the whole-cell pipette. Images were taken at 15 Hz using the Olympus Disk Spinning Unit Imaging System. After raw fluorescent signals from selected regions of interest (ROIs) were background subtracted at each time point, Ca^{2+} transients were expressed as $\Delta F/F_0 = (F(t) - F_0)/F_0$, where F_0 was determined as an average of $F(t)$ over a 1 s baseline period. Brief artifacts accompanying UV flashes are omitted from the fluorescence traces in flash photolysis experiments.

Drugs

Apamin, iberiotoxin, cyclopiazonic acid, DHPG, (*S*)-(+)-α -amino-4-carboxy-2-methylbenzeneacetic acid (LY367385), MPEP, DNQX, and picrotoxin were obtained from Tocris Biosciences. TTX was obtained from Alomone Labs. Fluo-4, Fluo-5F, and Fluo-4FF were purchased from Invitrogen. Caffeine, heparin sodium salt (from porcine intestinal mucosa), and muscarine chloride were obtained from Sigma RBI. Caged IP_3 was a generous gift from Dr. Kamran Khodakhah (Albert Einstein College of Medicine, Bronx, NY).

Data analysis

AP parameters were obtained from the first APs evoked during depolarizing current injections. AP threshold was determined as the point where the first derivative of the membrane potential (dv/dt) exceeded 20 V/s. AP half-width was measured at the potential halfway between AP threshold and peak. AHP amplitude was determined as the amount of hyperpolarization from AP threshold.

Data are expressed as mean ± SEM. Statistical significance was determined by Student's t test or ANOVA followed by Bonferroni *post hoc* test. The difference was considered significant at $p < 0.05$.

Results

Transient mGluR and mAChR stimulation inhibits SPN activity and activates SK and BK channels

To examine the effects of transient mGluR and mAChR activation on the firing of SPNs, whole-cell current-clamp recordings of these neurons were made in the dorsal striatum and AP firing was evoked by depolarizing current injections (200–350 pA; adjusted to produce ~5–7 Hz firing). Local pressure ejection (500 ms) of the group I mGluR (mGluR1/5) agonist DHPG (100 μM in a pipette placed ~50–80 μm from the recorded cell) produced a transient hyperpolarization and a pause in firing lasting 1.85 ± 0.11 s, followed by a delayed increase in the firing frequency, in eight cells tested (Fig. 1 *A*). When DHPG application was made at the resting membrane potential (approximately −80 to −95 mV) in six of these eight cells, no measurable response was observed. Pressure ejection of muscarine (100 μM; 500 ms), a broad-spectrum mAChR agonist, also caused membrane hyper-polarization and a pause in SPN firing (1.38 ± 0.15 s; $n = 5$), followed by gradual acceleration of firing (Fig. 1 *B*).

In voltage clamp (V_h =−57 mV), pressure ejection of DHPG (100 μM, 500 ms, once a minute) produced transient outward currents (~1–2 s), which were followed by prolonged inward currents (~20–50 s) (Fig. 1*C*). Bath perfusion of the mGluR1 antagonist LY367385 (75 nM) and the mGluR5 antagonist MPEP (50 nM) suppressed DHPG-induced outward currents (termed I_{DHPG}) by 47 ± 9 and 40 ± 8%, respectively, in six cells where these two antagonists were sequentially applied (three cells: LY367385 →MPEP +LY367385; three cells: MPEP →LY367385 + MPEP), indicating that these two mGluR subtypes make relatively equal contributions. LY367385 and MPEP similarly inhibited DHPG-induced delayed inward currents by 44 ±7 and 51 ± 6%, respectively. Pressure ejection of muscarine also produced transient outward currents followed by inward currents, which were abolished by the general mAChR antagonist atropine (2 μM) ($n = 3$; Fig. 1 *D*).

Group I mGluRs and mAChRs are coupled to Ca^{2+} -activated SK channels in many different types of neurons in other brain areas (Fiorillo and Williams, 2000; Morikawa et al., 2003; Gulledge and Stuart, 2005; Hagenston et al., 2008; Power and Sah, 2008; El-Hassar et al., 2011) and to BK channels in cerebellar Purkinje neurons (Canepari and Ogden, 2006). Indeed, I_{DHPG} amplitude was dramatically reduced when the holding potential was hyperpolarized to −87 mV (Fig. 1 *E*), consistent with the involvement of K^+ conductance. Thus, we examined the effects of the SK channel blocker apamin (100 nM) and the BK channel blocker iberiotoxin (IbTX) (100 nM) on I_{DHPG}. Apamin and IbTX reduced the peak amplitude of I_{DHPG} by 75 ± 4 and 26 ± 3%, respectively, and combined application of apamin and IbTX eliminated I_{DHPG} without affecting delayed inward currents ($n = 5$; three cells: apamin → IbTX + apamin; two cells: IbTX → apamin + IbTX) (Fig. 1 *F*). Accordingly, the apamin-sensitive SK-dependent component accounted for the majority (80 ± 4%) of charge transfer mediating I_{DHPG} (Fig. 1*G*). SK- and BK-dependent components reached their peak amplitude with similar latency after DHPG application, suggesting that

both types of Ca^{2+} -gated channels may be activated by the same Ca^{2+} signals. Therefore, transient activation of mGluR1/5 and mAChRs activates Ca^{2+}-sensitive SK and BK channels to regulate SPN excitability. DHPG- and muscarine-induced delayed inward currents were also depressed by membrane hyperpolarization (Fig. 1 *E*), suggesting that they result from closure of K^+ conductance.

IP_3R-dependent Ca^{2+} release from intracellular stores mediates SPN inhibition

When intracellular Ca^{2+} ($[Ca^{2+}]_i$) was monitored at the soma with the low-affinity (K_d = 9.7 μM) indicator Fluo-4FF (100 μM), local pressure ejection of DHPG produced a rise in $[Ca^{2+}]_i$ that coincided with I_{DHPG} (n = 7) (Fig. 2 *A*). We next made rapid application of IP_3 directly into the cytosol using UV photolysis of caged IP_3 (400 μM; dialyzed into the cytosol through the whole-cell pipette). Photolytic IP_3 application produced a transient rise in $[Ca^{2+}]_i$ and an outward current (termed I_{IP3}) in a concentration-dependent manner when three different UV flash intensities (50, 100, and 200 μJ) were used to vary the amount of IP_3 released (n = 3) (Fig. 2 *B*). Furthermore, intracellular application of heparin (1 mg/ml; whole-cell dialysis), an IP_3R antagonist (Ghosh et al., 1988), or bath application of cyclopiazonic acid (CPA) (20 μM), which depletes intracellular Ca^{2+} stores (Seidler et al., 1989), completely abolished both I_{DHPG} and I_{IP3} without affecting DHPG-induced delayed inward currents (Fig. 2*C–F*; recordings made with standard internal solution containing 25 μM EGTA). CPA also eliminated DHPG- and muscarine-induced suppression of SPN firing (n = 4 and 3, respectively) (Fig. 2*G*).

We further made detailed analyses of I_{IP3}, since flash photolysis of caged IP_3 enables much more quantitative and temporally precise application of IP_3 compared with local pressure ejection of DHPG or muscarine. I_{IP3} displayed concentration-dependent (i.e., UV flash intensity-dependent) increases in total charge transfer (termed Q_{IP3}) and half-width and a reduction in onset latency, accompanied by the emergence of an initial transient component with higher UV flash intensities (100–200 μJ) (n =5) (Fig. 3*A–C*). We next replaced EGTA in the internal solution with the same concentration (25 μM) of BAPTA (n = 5). Although these two Ca^{2+} buffers have similar steady-state affinities for Ca^{2+} (K_d = ~0.2 μM), thus similarly affecting baseline $[Ca^{2+}]_i$, BAPTA is much more effective in disrupting transient localized Ca^{2+} signaling processes due to its faster Ca^{2+} binding rate (~40–150 times) compared with EGTA (Fakler and Adelman, 2008; Eggermann et al., 2011). BAPTA (25 μM) reduced Q_{IP3} and half-width of I_{IP3} (measured at half the peak amplitude of the slow component) evoked by the highest UV intensity (200 μJ); however, it had no significant effect on the onset latency or the peak amplitudes of the initial or slow components. Increasing the BAPTA concentration to 1 mM completely eliminated I_{IP3} (n = 4), whereas measurable I_{IP3} was still observed with 1 mM EGTA (n = 4) (Fig. 3*D*). These data suggest that localized Ca^{2+} signaling is involved in the generation of I_{IP3}, presumably at the level of CICR among neighboring IP_3Rs that acts to sustain IP_3-induced Ca^{2+} rises.

When apamin and IbTX were tested onI_{IP3} (200 μJ UV intensity), SK- and BK-dependent components accounted for 78 ± 7 and 22 ± 7% of Q_{IP3}, respectively (n = 5; three cells: apamin →IbTX +apamin; two cells: IbTX → apamin + IbTX) (Fig. 4*A*). The initial fast component was mostly BK-mediated, suggesting that certain population of BK channels may have more direct access to IP_3R-mediated Ca^{2+} release. Small IP_3-induced inward currents were observed in the presence of apamin and IbTX. These inward currents became larger with membrane hyperpolarization to −87 mV (12.9 ± 1.6 pA at −57 mV vs 26.4 ± 2.0 pA at −87 mV, n =7; $t_{(6)}$ = 7.60, p < 0.001, paired t test), suggesting the involvement of a Ca^{2+} -activated cationic conductance (Fleig and Penner, 2004). Stable IP_3-induced currents were observed with repeated IP_3 applications (once a minute) even when recorded cells were constantly held at −87 mV (n = 5), indicating that Ca^{2+} stores can be replenished without

VGCC-mediated Ca^{2+} influx (i.e., priming) in SPNs (Hong and Ross, 2007; Wu et al., 2011).

In current clamp, photolytic IP_3 application produced a pause in SPN firing (0.68 ± 0.03 s; n = 9). Apamin and IbTX reduced the duration of this IP_3-induced pause by 47 ± 5% (n = 4) and 22 ± 9% (n = 5), respectively, while combined application of apamin and IbTX eliminated the pause (n = 3) (Fig. 4 *B–D*). IP_3 application produced small depolarizations at the resting membrane potential (1.8 ± 0.1 mV; n = 10), consistent with the cationic conductance described above.

Together, these data indicate that IP_3R-mediated Ca^{2+} release from intracellular stores, causing activation of SK and BK channels, is responsible for mGluR- and mAChR-induced inhibition of SPNs.

Synaptic stimulation triggers mGluR-and mAChR-mediated IPSCs

We next examined synaptic responses (AMPA, NMDA, and $GABA_A$ receptors blocked) elicited by intrastriatal stimulation using a bipolar stimulating electrode (~600 μm tip separation) placed caudal to the recorded cell (~500–600 μm away) (Fig. 5*A*). This likely causes stimulation of a large number of inputs arising from all available sources, both intrinsic fibers from striatal neurons and extrinsic inputs from other structures, including those from the cortex via antidromic stimulation (Cowan and Wilson, 1994). Although single stimuli (500 μs; ~1–2 mA) failed to produce measurable responses, trains of 2–10 stimuli at 50 Hz evoked slow IPSC-like outward currents (V_h = −57 mV) (Fig. 5*B*). A train of 5 stimuli produced a near-saturating response in four cells tested for various train lengths (1–10 stimuli), and hence were used in the following experiments. IPSC-like outward currents thus evoked, which peaked at 0.47 ± 0.03 s after the onset of stimulus train and had a half-width of 0.58 ± 0.03 s (n =14), were largely suppressed by CPA (20 μM; n =4) and also by combined application of LY367385 (mGluR1 antagonist; 75 nM), MPEP (mGluR5 antagonist; 50 nM), and atropine (mAChR antagonist; 2 μM) (n =10) (Fig. 5*C,D*), indicating that they mostly represent Ca^{2+} store-dependent mGluR/mAChR IPSCs. Small outward currents (~10 pA or less) routinely remained after application of CPA or the mGluR/mAChR antagonist mixture. The outward currents in the presence of antagonist mixture were not suppressed by subsequent application of CPA (n = 3) or the $GABA_B$ receptor antagonist CGP54626 [[*S*-(*R**,*R**)]-[3-[[1-(3,4-dichlorophenyl) ethyl]amino]-2-hydroxypropyl](cyclohexylmethyl) phosphinic acid] (1 μM; n =3), and thus their identity is currently unknown. On average, mGluR- and mAChR-mediated components made equal contributions to IPSCs, while mGluR1 accounted for the vast majority of the mGluR-dependent component. All 10 cells examined had both mGluR- and mAChR-mediated components, although the relative size varied from cell to cell. These results demonstrate that synaptic stimulation of glutamatergic and cholinergic inputs produces Ca^{2+} store-dependent inhibition of SPNs. Delayed EPSCs (~10 pA) sensitive to atropine were observed in 3 of 14 cells.

RyR-dependent, but IP_3R-independent, Ca^{2+}release contributes to slow AHPs

It has been shown that AP-evoked Ca^{2+} influx activates BK and SK channels, thereby producing fast and slow AHPs (fAHPs and sAHPs) in SPNs (Pineda et al., 1992; Hopf et al., 2010). In line with these studies, IbTX increased the AP half-width and suppressed fAHPs (peaked at ~2–3 ms after AP onset) without affecting the interspike interval (n = 6), indicating the role of BK channels in AP repolarization, whereas apamin depressed sAHPs (peaked at ~20–40 ms after AP onset) and decreased the inter-spike interval (n = 6) (Fig. 6 *A*, *B*; Table 1). CICR from intracellular stores triggered by AP-evoked Ca^{2+} influx may contribute to sAHPs (Berridge, 1998). We found that Ca^{2+} store depletion with CPA

dramatically suppressed sAHPs and decreased the interspike interval ($n = 8$), an effect that was occluded by previous application of apamin ($n = 4$) (Fig. 6*C*, Table 1). Therefore, CICR contributes to SK-dependent sAHPs in SPNs. Apamin and CPA also accelerated the initial ramp-like depolarizations preceding the first AP during depolarizing current injections, demonstrating that CICR-dependent SK channel activation, in addition to activation of voltage-gated K^+ conductances (Nisenbaum and Wilson, 1995), is capable of delaying the firing response to depolarizing inputs.

We next measured the currents underlying sAHPs in voltage clamp, as has been done previously in midbrain dopamine neurons and striatal cholinergic interneurons (Goldberg and Wilson, 2005; Cui et al., 2007). Here, 2 ms depolarizing pulses to −7 mV from a holding potential of −57 mV were applied to evoke un-clamped APs, which resulted in tail outward currents (I_{sAHP}) lasting ~200 ms (Fig. 7*A*). We calculated the time integral of I_{sAHP} (i.e., the total charge transfer) after removing a 10 ms window following the 2 ms depolarizing pulse. Q_{sAHP} thus obtained was largely suppressed (87 ± 2%; $n = 4$) by TTX (1 μM), consistent with the role of unclamped APs in generating I_{sAHP}. Apamin and IbTX reduced Q_{sAHP} by 76 ± 5 and 10 ± 3%, respectively ($n = 5$; three cells: apamin →IbTX + apamin; two cells: IbTX → apamin + IbTX) (Fig. 7 *B*, *C*). Ca^{2+} store depletion with CPA depressed Q_{AHP} by 56 ± 7% ($n = 5$) (Fig. 7 *D*, *E*). Furthermore, prior application of CPA dramatically reduced the SK-dependent component of Q_{sAHP} and eliminated the small BK-dependent component ($n = 4$) (Fig. 7*C*,*E*). Thus, CICR-dependent activation of SK channels largely mediates I_{sAHP} evoked by un-clamped APs, consistent with its dominant role in controlling sAHPs and interspike interval during depolarization-induced firing described above (Fig. 6, Table 1).

AP-induced CICR that mediates sAHPs frequently occurs via RyRs (Sah and McLachlan, 1991; Kakizawa et al., 2007), although IP_3Rs may also play a role (Cui et al., 2007). We next recorded I_{sAHP} with heparin (1 mg/ml) in the recording pipette to test the involvement of IP_3Rs. Heparin, which abolished I_{DHPG} and I_{IP3} in ~5 min (Fig. 2*C*,*D*), had no effect on Q_{sAHP} ($n = 5$) (Fig. 7*F*). Furthermore, it failed to suppress CPA-induced depression of Q_{sAHP} (55 ± 8%, $n = 5$; $p = 0.94$ vs CPA effect with control internal solution, unpaired *t* test). Therefore, IP_3Rs are not involved in the CICR-dependent component of sAHPs.

To examine the involvement of RyRs, we used caffeine, which increases the Ca^{2+} sensitivity of RyRs while at the same time blocks IP_3Rs (Ehrlich et al., 1994). Bath application of caffeine (1 and 2 mM) reversibly increased Q_{sAHP} but depressed I_{IP3} and I_{DHPG} in a concentration-dependent manner (Fig. 8 *A*, *B*). We further tested the effect of ryanodine (20 μM), which locks RyR channels in a subconductance open state and thus depletes Ca^{2+} stores expressing RyRs (Zucchi and Ronca-Testoni, 1997). Ryanodine inhibited Q_{sAHP} by 56 ± 8% ($n = 5$), an inhibition virtually identical with that produced by CPA, and completely abolished I_{IP3} (Fig. 8*C*). These data demonstrate that, although IP_3Rs and RyRs are coexpressed on the same Ca^{2+} stores, these two Ca^{2+} release channels are functionally segregated, where IP_3 selectively elicits IP_3R-mediated Ca^{2+}release, without invoking CICR via RyRs, to mediate mGluR/mAChR-induced inhibition of SPN activity, whereas AP-induced Ca^{2+} influx through VGCCs selectively recruits RyR-mediated Ca^{2+} release to generate sAHPs (Fig. 8 *D*). Ca^{2+} influx through certain types of VGCCs at depolarized potentials may enlarge the size of Ca^{2+} stores (Power and Sah, 2005) or enhance the activity of PLC (Nevian and Sakmann, 2006); however, we found that bath application of the general VGCC blocker Cd^{2+} (100 μM), which suppressed Q_{sAHP} by 78 ± 1% ($n = 3$), had no significant effect on I_{DHPG} measured at −57 mV ($n = 4$) (Fig. 8 *E*), further confirming that Ca^{2+} stores can be maintained without VGCC-mediated Ca^{2+} influx in SPNs.

We next tested EGTA/BAPTA sensitivity of SK- and BK-dependent components of I_{sAHP} (I_{sAHP}-SK and I_{sAHP}-BK) (Fig. 9). Replacing 25 μM EGTA with 25 μM BAPTA depressed I_{sAHP}-SK, without changing its half-width, and abolished I_{sAHP}-BK. Increasing the BAPTA concentration to 1 mM virtually eliminated I_{sAHP}-SK, while measurable I_{sAHP}-SK was observed with 1 mM EGTA, although reduced in size compared with that in 25 μM EGTA. Thus, both components were more sensitive to BAPTA than to EGTA, implying the involvement of localized Ca^{2+} signaling processes. The higher sensitivity of I_{sAHP}-BK to these Ca^{2+} buffers compared with I_{sAHP}-SK likely reflects different Ca^{2+} sensitivity of BK versus SK channels.

IP_3-induced Ca^{2+} signaling is absent in striatal interneurons

A previous immunohistochemical study has shown that expression of neuronal type 1 IP_3Rs is restricted to SPNs in the striatum, with little or no IP_3R expression in other aspiny neurons, particularly in cholinergic neurons and parvalbumin-containing neurons, whereas RyRs are expressed in virtually all striatal neurons (Martone et al., 1997). In agreement with this study, flash photolysis of caged IP_3 (400 μM; ~200 μJ UV intensity), as well as trains of 5–10 unclamped APs at 20 Hz, invariably produced robust Ca^{2+} transients in all SPNs tested [nine cells with 100 μM Fluo-4FF (K_d = 9.7 μM), two cells with 100 μM Fluo-5F (K_d = 2.3 μM), one cell with 200 μM Fluo-4 (K_d = 0.35 μM)] (Fig. 10 *A*). In contrast, the same photolytic application of IP_3 failed to evoke detectable Ca^{2+} rises in electrophysiologically identified cholinergic interneurons (ChIs) (n = 4), fast-spiking interneurons (FSIs) (n =3), and low-threshold spike (LTS) interneurons (n = 3) even when $[Ca^{2+}]_i$ was monitored with the high-affinity indicator Fluo-4 (200 μM), while trains of unclamped APs (ChIs and LTS neurons: 5 APs at 10 Hz; FSIs: 5–10 APs at 20 Hz) were capable of producing Ca^{2+} transients (Fig. 10 *B–D*). When recordings were made with our routine internal solution containing 25 μM EGTA (without Ca^{2+} indicators), IP_3 application elicited no measurable currents, while unclamped APs evoked apamin-sensitive I_{sAHP}, in ChIs (n = 4) and LTS neurons (n = 3; IP_3 tested in two of these three cells) (Fig. 10*E*). No IP_3-evoked currents or I_{sAHP} were observed in FSIs (n = 5) (data not shown). These data strongly suggest that functional IP_3Rs are selectively expressed in SPNs among different types of striatal neurons.

Discussion

Inhibitory regulation of SPN activity is thought to be achieved either through feedback inhibition among SPNs or via feedforward inhibition by GABAergic interneurons, recruited by extrinsic glutamatergic and local cholinergic inputs (Ponzi and Wickens, 2010; English et al., 2012; Gittis and Kreitzer, 2012). Here, we found that glutamatergic and cholinergic inputs can directly inhibit SPNs via mGluR/mAChR-induced intracellular Ca^{2+} release and subsequent activation of SK and BK channels. IP_3Rs are selectively involved in mGluR/mAChR-induced Ca^{2+} release without playing a role in CICR triggered by AP-evoked Ca^{2+} influx. Intriguingly, IP_3-induced Ca^{2+} release is not observed in striatal interneurons. Therefore, IP_3 signaling is uniquely involved in glutamatergic and cholinergic inhibition of striatal output neuron activity.

Mechanisms of mGluR- and mAChR-induced inhibition

Both local pressure ejection of agonists and intrastriatal stimulation of glutamatergic and cholinergic inputs produce Ca^{2+} store-dependent inhibitory responses in SPNs. Experiments were mostly performed in the presence of the $GABA_A$ blocker picrotoxin, ruling out the contribution of local GABAergic network. Curiously, the mGluR-dependent component of IPSCs is almost exclusively mediated by the mGluR1 subtype, while pressure ejection of DHPG, which would reach an area surrounding the soma, proximal dendrites, and maybe

part of more distal dendrites equipped with spines, equally engages both mGluR1 and mGluR5. Previous ultrastructural studies in SPNs have shown that both mGluR1 and mGluR5 are equally distributed on dendritic spines and shafts, mostly at extrasynaptic sites, although mGluR5 is more frequently detected than mGluR1 at the soma (Paquet and Smith, 2003; Mitrano and Smith, 2007). Pharmacologically, these two mGluR subtypes have similar affinities to glutamate as well as to DHPG (Schoepp et al., 1999). Therefore, it is not clear why mGluR5-dependent IPSCs were not detected. Of note, distinct roles of mGluR1 versus mGluR5 on AMPA/NMDA-mediated glutamatergic transmission and plasticity have been reported in SPNs (Gubellini et al., 2004). It remains to be determined how these two mGluR subtypes differentially sense synaptically released glutamate and signal its consequence.

mAChR-dependent inhibitory responses are most likely mediated by the PLC-coupled M_1 subtype, which is expressed in virtually all SPNs (Yan et al., 2001). The majority of cholinergic terminals in the striatum, which arise from ChIs, do not make synaptic contacts onto other neurons (Contant et al., 1996). This, together with the extrasynaptic localization of mGluRs described above, may account for the requirement of repetitive, high-frequency stimulation to elicit IPSCs via extrasynaptic diffusion of glutamate/ACh (Brasnjo and Otis, 2001). mAChR-dependent inhibition may contribute, in part, to the suppression of SPN firing caused by selective excitation of ChIs *in vivo* (Witten et al., 2010; English et al., 2012).

SK channels and, to a smaller degree, BK channels both contribute to mGluR-and IP_3-induced outward currents. mGluR/mAChR/IP_3-induced outward currents/hyperpolarizations are entirely mediated by SK channels in cortical pyramidal neurons (Gulledge and Stuart, 2005; Hagenston et al., 2008), hippocampal CA1 pyramidal neurons (El-Hassar et al., 2011), basolateral amygdala (BLA) neurons (Power and Sah, 2008), and midbrain dopamine neurons (Fiorillo and Williams, 2000; Morikawa et al., 2000, 2003). In contrast, mGluR/IP_3-induced Ca^{2+} signaling is exclusively coupled to BK channels in cerebellar Purkinje neurons (Khodakhah and Ogden, 1995; Canepari and Ogden, 2006), even though these neurons express SK channels (Womack and Khodakhah, 2003). SK channels are solely gated by Ca^{2+} with submicromolar affinity, while BK channels are gated by voltage and Ca^{2+} (Fakler and Adelman, 2008). Both strong depolarization (≥0 mV) and very high $[Ca^{2+}]_i$ (≥10 μM) are generally necessary to activate BK channels. This large difference in Ca^{2+} sensitivity readily accounts for the major contribution of SK channels at rather hyperpolarized potentials (below −50 mV) in many neurons described above. However, recent evidence indicates that BK channel gating is dramatically enhanced by auxiliary proteins, termed LRRC (leucine-rich repeat-containing) proteins, which allow BK channel activation by submicromolar to micromolar $[Ca^{2+}]_i$ even at hyperpolarized potentials (Yan and Aldrich, 2010, 2012). mRNAs of these proteins are found in the brain, raising the possibility that certain BK channels might have high Ca^{2+} sensitivity in neurons. Indeed, BK- and SK-dependent components of I_{DHPG} and I_{IP3} had similar kinetics (except for the initial BK component of I_{IP3}), suggesting that these two Ca^{2+} -activated channels may be sensing the same Ca^{2+} signals in SPNs.

As in cortical and hippocampal pyramidal neurons and BLA neurons (Power and Sah, 2002, 2005; Gulledge and Stuart, 2005; Hagenston et al., 2008), mGluR-induced, and likely mAChR-induced, Ca^{2+} signaling in SPNs is entirely dependent on IP_3-mediated Ca^{2+} release, boosted by CICR among neighboring IP_3Rs without recruiting CICR via RyRs. Both IP_3Rs and RyRs are involved in mGluR-induced Ca^{2+} release in dopamine neurons; however, these two Ca^{2+} release mechanisms occur independently, being mediated by distinct intracellular second messengers, IP_3 for IP_3Rs and cyclic ADP-ribose for RyRs (Morikawa et al., 2003). Therefore, IP_3Rs and RyRs generally exhibit functional

segregation, although these two Ca^{2+} release channels have been shown to be coexpressed on the same pool of Ca^{2+} stores in all of these neurons, consistent with the idea that endoplasmic reticulum Ca^{2+} stores form a single continuous network in individual cells (Berridge, 1998). Functional segregation of IP_3Rs and RyRs may, at least partially, be accounted for by their differential subcellular localization (Sharp et al., 1993).

mGluR/mAChR activation also produces an inward current independent of Ca^{2+} release in SPNs. This most likely results from closure of KCNQ K^+ channels as a consequence of PLC-dependent depletion of a membrane phospholipid, phosphatidylinositol 4,5-bisphosphate (Shen et al., 2005). In contrast, photolytic application of IP_3 causes a transient inward current, which is likely due to a TRPC-like cationic conductance activated by Ca^{2+} (Zhu, 2005). mGluR/mAChR-induced excitatory responses observed in many different neurons generally depend on either, or both, of these two ionic mechanisms (Fiorillo and Williams, 2000; Gulledge and Stuart, 2005; Canepari and Ogden, 2006; Hagenston et al., 2008; El-Hassar et al., 2011). The amount and spatiotemporal profile of IP_3 achieved by mGluR/mAChR activation appears to be insufficient to activate TRPC-like channels in SPNs.

Ca^{2+} store dependence of slow AHPs

BK and SK channels make distinct contributions to different phases of AHPs (Fakler and Adelman, 2008). Indeed, BK and SK channels contribute to fAHPs and sAHPs, respectively, in SPNs. Our data further demonstrate that sAHPs are largely dependent on intracellular Ca^{2+} release. I_{sAHP} evoked by unclamped APs was augmented by caffeine, which increases Ca^{2+} sensitivity of RyRs, but unaffected by heparin, an IP_3R antagonist. Thus, RyR-dependent CICR triggered by AP-induced Ca^{2+} influx accounts for the Ca^{2+} store dependence of sAHPs, as in other neurons (Sah and McLachlan, 1991; Berridge, 1998; Kakizawa et al., 2007). This is also in line with the preferential localization of RyRs at the soma and proximal dendrites in SPNs (Martone et al., 1997), which display limited backpropagation of APs into distal dendrites (Day et al., 2008). However, AP-induced Ca^{2+} influx can trigger IP_3R-dependent CICR when IP_3 levels are elevated by activation of mGluRs and other PLC-coupled receptors in cortical and hippocampal pyramidal neurons (Nakamura et al., 2000; Stutzmann et al., 2003), BLA neurons (Power and Sah, 2008), and dopamine neurons (Cui et al., 2007). It remains to be determined whether similar “cross talk” of AP-induced Ca^{2+} influx and IP_3 signaling occurs in SPNs.

I_{sAHP} had a small BK component, while the BK channel blocker IbTX failed to affect sAHPs. A small reduction in BK-dependent sAHPs might be offset by IbTX-induced AP broadening, which would augment AP-evoked Ca^{2+} influx and subsequent SK channel activation. Based on differential sensitivity to EGTA and BAPTA, localized Ca^{2+} signaling around VGCCs is thought to drive BK channel activation that mediates AP repolarization and fAHPs (Fakler and Adelman, 2008). Our data suggest that the Ca^{2+} store-dependent component of sAHPs also involves highly BAPTA-sensitive, localized Ca^{2+} signaling, from RyRs to SK/BK channels and/or from VGCCs to RyRs, in SPNs (Fig. 7*D*).

IP_3-induced Ca^{2+} signaling selectively regulates SPNs in the striatum

All SPNs showed robust responses to DHPG, muscarine, or IP_3 applications. In contrast, striatal interneurons failed to respond to photolytic IP_3 application using maximal UV intensity used in the present study, in agreement with an immunohistochemical study reporting selective expression of IP_3Rs in SPNs among striatal neurons (Martone et al., 1997). To our knowledge, this is the first indication that functional IP_3 signaling is specific to projection neurons in a given brain area, although we cannot completely rule out the possibility that striatal interneurons might express IP_3Rs with extremely low sensitivity.

SPNs fire clusters of APs interrupted by periods of pauses *in vivo*, sometimes without transition to a full DOWN state (Wilson and Kawaguchi, 1996; Stern et al., 1998). Firing pauses in distinct populations of SPNs are thought to be important for action selection and deselection (Jin and Costa, 2010; Krause et al., 2010). Working in concert with feedback and feedforward GABAergic mechanisms, robust IP_3-mediated inhibition driven by glutamatergic and cholinergic inputs onto SPNs themselves might contribute to these pauses observed in behaving animals.

Acknowledgments

This work was supported by NIH Grants DA015687 and AA015521. We thank Dr. Kamran Khodakhah for the generous gift of caged IP_3 made in his laboratory. We also thank Dr. Mark Harnett for critical comments on this manuscript.

References

Berridge MJ. Neuronal calcium signaling. Neuron. 1998; 21:13–26. [PubMed: 9697848]

Brasnjo G, Otis TS. Neuronal glutamate transporters control activation of postsynaptic metabotropic glutamate receptors and influence cerebellar long-term depression. Neuron. 2001; 31:607–616. [PubMed: 11545719]

Canepari M, Ogden D. Kinetic, pharmacological and activity-dependent separation of two Ca^{2+} signalling pathways mediated by type 1 metabotropic glutamate receptors in rat Purkinje neurones. J Physiol. 2006; 573:65–82. [PubMed: 16497716]

Contant C, Umbriaco D, Garcia S, Watkins KC, Descarries L. Ultra-structural characterization of the acetylcholine innervation in adult rat neostriatum. Neuroscience. 1996; 71:937–947. [PubMed: 8684624]

Cowan RL, Wilson CJ. Spontaneous firing patterns and axonal projections of single corticostriatal neurons in the rat medial agranular cortex. J Neurophysiol. 1994; 71:17–32. [PubMed: 8158226]

Cui G, Bernier BE, Harnett MT, Morikawa H. Differential regulation of action potential- and metabotropic glutamate receptor-induced Ca^{2+} signals by inositol 1,4,5-trisphosphate in dopaminergic neurons. J Neurosci. 2007; 27:4776–4785. [PubMed: 17460090]

Day M, Wokosin D, Plotkin JL, Tian X, Surmeier DJ. Differential excitability and modulation of striatal medium spiny neuron dendrites. J Neurosci. 2008; 28:11603–11614. [PubMed: 18987196]

Eggermann E, Bucurenciu I, Goswami SP, Jonas P. Nanodomain coupling between Ca^{2+} channels and sensors of exocytosis at fast mammalian synapses. Nat Rev Neurosci. 2012; 13:7–21. [PubMed: 22183436]

Ehrlich BE, Kaftan E, Bezprozvannaya S, Bezprozvanny I. The pharmacology of intracellular Ca^{2+}-release channels. Trends Pharmacol Sci. 1994; 15:145–149. [PubMed: 7754532]

El-Hassar L, Hagenston AM, D'Angelo LB, Yeckel MF. Metabotropic glutamate receptors regulate hippocampal CA1 pyramidal neuron excitability via Ca^{2+} wave-dependent activation of SK and TRPC channels. J Physiol. 2011; 589:3211–3229. [PubMed: 21576272]

English DF, Ibanez-Sandoval O, Stark E, Tecuapetla F, Buzsáki G, Deisseroth K, Tepper JM, Koos T. GABAergic circuits mediate the reinforcement-related signals of striatal cholinergic interneurons. Nat Neurosci. 2012; 15:123–130. [PubMed: 22158514]

Fakler B, Adelman JP. Control of K(Ca) channels by calcium nano/microdomains. Neuron. 2008; 59:873–881. [PubMed: 18817728]

Fiorillo CD, Williams JT. Cholinergic inhibition of ventral midbrain dopamine neurons. J Neurosci. 2000; 20:7855–7860. [PubMed: 11027251]

Fleig A, Penner R. The TRPM ion channel subfamily: molecular, biophysical and functional features. Trends Pharmacol Sci. 2004; 25:633–639. [PubMed: 15530641]

Ghosh TK, Eis PS, Mullaney JM, Ebert CL, Gill DL. Competitive, reversible, and potent antagonism of inositol 1,4,5-trisphosphate-activated calcium release by heparin. J Biol Chem. 1988; 263:11075–11079. [PubMed: 3136153]

Gittis AH, Kreitzer AC. Striatal microcircuitry and movement disorders. Trends Neurosci. 2012; 35:557–564. [PubMed: 22858522]

Goldberg JA, Wilson CJ. Control of spontaneous firing patterns by the selective coupling of calcium currents to calcium-activated potassium currents in striatal cholinergic interneurons. J Neurosci. 2005; 25:10230–10238. [PubMed: 16267230]

Graybiel AM, Aosaki T, Flaherty AW, Kimura M. The basal ganglia and adaptive motor control. Science. 1994; 265:1826–1831. [PubMed: 8091209]

Gubellini P, Pisani A, Centonze D, Bernardi G, Calabresi P. Metabotropic glutamate receptors and striatal synaptic plasticity: implications for neurological diseases. Prog Neurobiol. 2004; 74:271–300. [PubMed: 15582223]

Gulledge AT, Stuart GJ. Cholinergic inhibition of neocortical pyramidal neurons. J Neurosci. 2005; 25:10308–10320. [PubMed: 16267239]

Hagenston AM, Fitzpatrick JS, Yeckel MF. MGluR-mediated calcium waves that invade the soma regulate firing in layer V medial prefrontal cortical pyramidal neurons. Cereb Cortex. 2008; 18:407–423. [PubMed: 17573372]

Hikosaka O, Sakamoto M, Usui S. Functional properties of monkey caudate neurons. III. Activities related to expectation of target and reward. J Neurophysiol. 1989; 61:814–832. [PubMed: 2723722]

Hong M, Ross WN. Priming of intracellular calcium stores in rat CA1 pyramidal neurons. J Physiol. 2007; 584:75–87. [PubMed: 17690146]

Hopf FW, Seif T, Mohamedi ML, Chen BT, Bonci A. The small-conductance calcium-activated potassium channel is a key modulator of firing and long-term depression in the dorsal striatum. Eur J Neurosci. 2010; 31:1946–1959. [PubMed: 20497469]

Jin X, Costa RM. Start/stop signals emerge in nigrostriatal circuits during sequence learning. Nature. 2010; 466:457–462. [PubMed: 20651684]

Kakizawa S, Kishimoto Y, Hashimoto K, Miyazaki T, Furutani K, Shimizu H, Fukaya M, Nishi M, Sakagami H, Ikeda A, Kondo H, Kano M, Watanabe M, Iino M, Takeshima H. Junctophilin-mediated channel crosstalk essential for cerebellar synaptic plasticity. EMBO J. 2007; 26:1924–1933. [PubMed: 17347645]

Kawaguchi Y. Physiological, morphological, and histochemical characterization of three classes of interneurons in rat neostriatum. J Neurosci. 1993; 13:4908–4923. [PubMed: 7693897]

Khodakhah K, Ogden D. Fast activation and inactivation of inositol trisphosphate-evoked Ca^{2+} release in rat cerebellar Purkinje neurones. J Physiol. 1995; 487:343–358. [PubMed: 8558468]

Krause M, German PW, Taha SA, Fields HL. A pause in nucleus accumbens neuron firing is required to initiate and maintain feeding. J Neurosci. 2010; 30:4746–4756. [PubMed: 20357125]

Martone ME, Alba SA, Edelman VM, Airey JA, Ellisman MH. Distribution of inositol-1,4,5-trisphosphate and ryanodine receptors in rat neostriatum. Brain Res. 1997; 756:9–21. [PubMed: 9187309]

McCray JA, Herbette L, Kihara T, Trentham DR. A new approach to time-resolved studies of ATP-requiring biological systems; laser flash photolysis of caged ATP. Proc Natl Acad Sci U S A. 1980; 77:7237–7241. [PubMed: 6938971]

Mitrano DA, Smith Y. Comparative analysis of the subcellular and subsynaptic localization of mGluR1a and mGluR5 metabotropic glutamate receptors in the shell and core of the nucleus accumbens in rat and monkey. J Comp Neurol. 2007; 500:788–806. [PubMed: 17154259]

Morikawa H, Imani F, Khodakhah K, Williams JT. Inositol 1,4,5-triphosphate-evoked responses in midbrain dopamine neurons. J Neurosci. 2000; 20(1–5):RC103. [PubMed: 11027254]

Morikawa H, Khodakhah K, Williams JT. Two intracellular pathways mediate metabotropic glutamate receptor-induced Ca^{2+} mobilization in dopamine neurons. J Neurosci. 2003; 23:149–157. [PubMed: 12514211]

Nakamura T, Nakamura K, Lasser-Ross N, Barbara JG, Sandler VM, Ross WN. Inositol 1,4,5-trisphosphate (IP3)-mediated Ca^{2+} release evoked by metabotropic agonists and backpropagating action potentials in hippocampal CA1 pyramidal neurons. J Neurosci. 2000; 20:8365–8376. [PubMed: 11069943]

Nevian T, Sakmann B. Spine Ca^{2+} signaling in spike-timing-dependent plasticity. J Neurosci. 2006; 26:11001–11013. [PubMed: 17065442]

Nisenbaum ES, Wilson CJ. Potassium currents responsible for inward and outward rectification in rat neostriatal spiny projection neurons. J Neurosci. 1995; 15:4449–4463. [PubMed: 7790919]

Paquet M, Smith Y. Group I metabotropic glutamate receptors in the monkey striatum: subsynaptic association with glutamatergic and dopaminergic afferents. J Neurosci. 2003; 23:7659–7669. [PubMed: 12930805]

Pineda JC, Galarraga E, Bargas J, Cristancho M, Aceves J. Charybdotoxin and apamin sensitivity of the calcium-dependent repolarization and the afterhyperpolarization in neostriatal neurons. J Neurophysiol. 1992; 68:287–294. [PubMed: 1381420]

Ponzi A, Wickens J. Sequentially switching cell assemblies in random inhibitory networks of spiking neurons in the striatum. J Neurosci. 2010; 30:5894–5911. [PubMed: 20427650]

Power JM, Sah P. Nuclear calcium signaling evoked by cholinergic stimulation in hippocampal CA1 pyramidal neurons. J Neurosci. 2002; 22:3454–3462. [PubMed: 11978822]

Power JM, Sah P. Intracellular calcium store filling by an L-type calcium current in the basolateral amygdala at subthreshold membrane potentials. J Physiol. 2005; 562:439–453. [PubMed: 15550460]

Power JM, Sah P. Competition between calcium-activated K^+ channels determines cholinergic action on firing properties of basolateral amygdala projection neurons. J Neurosci. 2008; 28:3209–3220. [PubMed: 18354024]

Sah P, McLachlan EM. Ca^{2+}-activated K^+ currents underlying the afterhyperpolarization in guinea pig vagal neurons: a role for Ca^{2+}-activated Ca^{2+} release. Neuron. 1991; 7:257–264. [PubMed: 1873029]

Schoepp DD, Jane DE, Monn JA. Pharmacological agents acting at subtypes of metabotropic glutamate receptors. Neuropharmacology. 1999; 38:1431–1476. [PubMed: 10530808]

Seidler NW, Jona I, Vegh M, Martonosi A. Cyclopiazonic acid is a specific inhibitor of the Ca^{2+}-ATPase of sarcoplasmic reticulum. J Biol Chem. 1989; 264:17816–17823. [PubMed: 2530215]

Sharp AH, McPherson PS, Dawson TM, Aoki C, Campbell KP, Snyder SH. Differential immunohistochemical localization of inositol 1,4,5-trisphosphate- and ryanodine-sensitive Ca^{2+} release channels in rat brain. J Neurosci. 1993; 13:3051–3063. [PubMed: 8392539]

Shen W, Hamilton SE, Nathanson NM, Surmeier DJ. Cholinergic suppression of KCNQ channel currents enhances excitability of striatal medium spiny neurons. J Neurosci. 2005; 25:7449–7458. [PubMed: 16093396]

Stern EA, Jaeger D, Wilson CJ. Membrane potential synchrony of simultaneously recorded striatal spiny neurons in vivo. Nature. 1998; 394:475–478. [PubMed: 9697769]

Stutzmann GE, LaFerla FM, Parker I. Ca^{2+} signaling in mouse cortical neurons studied by two-photon imaging and photoreleased inositol triphosphate. J Neurosci. 2003; 23:758–765. [PubMed: 12574404]

Surmeier DJ, Ding J, Day M, Wang Z, Shen W. D1 and D2 dopamine-receptor modulation of striatal glutamatergic signaling in striatal medium spiny neurons. Trends Neurosci. 2007; 30:228–235. [PubMed: 17408758]

Tepper JM, Wilson CJ, Koós T. Feedforward and feedback inhibition in neostriatal GABAergic spiny neurons. Brain Res Rev. 2008; 58:272–281. [PubMed: 18054796]

Walker JW, Feeney J, Trentham DR. Photolabile precursors of inositol phosphates. Preparation and properties of 1-(2-nitrophenyl)ethyl esters of myoinositol 1,4,5-trisphosphate. Biochemistry. 1989; 28:3272–3280. [PubMed: 2787165]

Wilson CJ, Kawaguchi Y. The origins of two-state spontaneous membrane potential fluctuations of neostriatal spiny neurons. J Neurosci. 1996; 16:2397–2410. [PubMed: 8601819]

Witten IB, Lin SC, Brodsky M, Prakash R, Diester I, Anikeeva P, Gradinaru V, Ramakrishnan C, Deisseroth K. Cholinergic interneurons control local circuit activity and cocaine conditioning. Science. 2010; 330:1677–1681. [PubMed: 21164015]

Womack MD, Khodakhah K. Somatic and dendritic small-conductance calcium-activated potassium channels regulate the output of cerebellar Purkinje neurons. J Neurosci. 2003; 23:2600–2607. [PubMed: 12684445]

Wu J, Shih HP, Vigont V, Hrdlicka L, Diggins L, Singh C, Mahoney M, Chesworth R, Shapiro G, Zimina O, Chen X, Wu Q, Glushankova L, Ahlijanian M, Koenig G, Mozhayeva GN, Kaznacheyeva E, Bezprozvanny I. Neuronal store-operated calcium entry pathway as a novel therapeutic target for Huntington's disease treatment. Chem Biol. 2011; 18:777–793. [PubMed: 21700213]

Yan J, Aldrich RW. LRRC26 auxiliary protein allows BK channel activation at resting voltage without calcium. Nature. 2010; 466:513–516. [PubMed: 20613726]

Yan J, Aldrich RW. BK potassium channel modulation by leucine-rich repeat-containing proteins. Proc Natl Acad Sci U S A. 2012; 109:7917–7922. [PubMed: 22547800]

Yan Z, Flores-Hernandez J, Surmeier DJ. Coordinated expression of muscarinic receptor messenger RNAs in striatal medium spiny neurons. Neuroscience. 2001; 103:1017–1024. [PubMed: 11301208]

Zhu MX. Multiple roles of calmodulin and other Ca^{2+}-binding proteins in the functional regulation of TRP channels. Pflugers Arch. 2005; 451:105–115. [PubMed: 15924238]

Zucchi R, Ronca-Testoni S. The sarcoplasmic reticulum Ca^{2+} channel/ryanodine receptor: modulation by endogenous effectors, drugs and disease states. Pharmacol Rev. 1997; 49:1–51. [PubMed: 9085308]

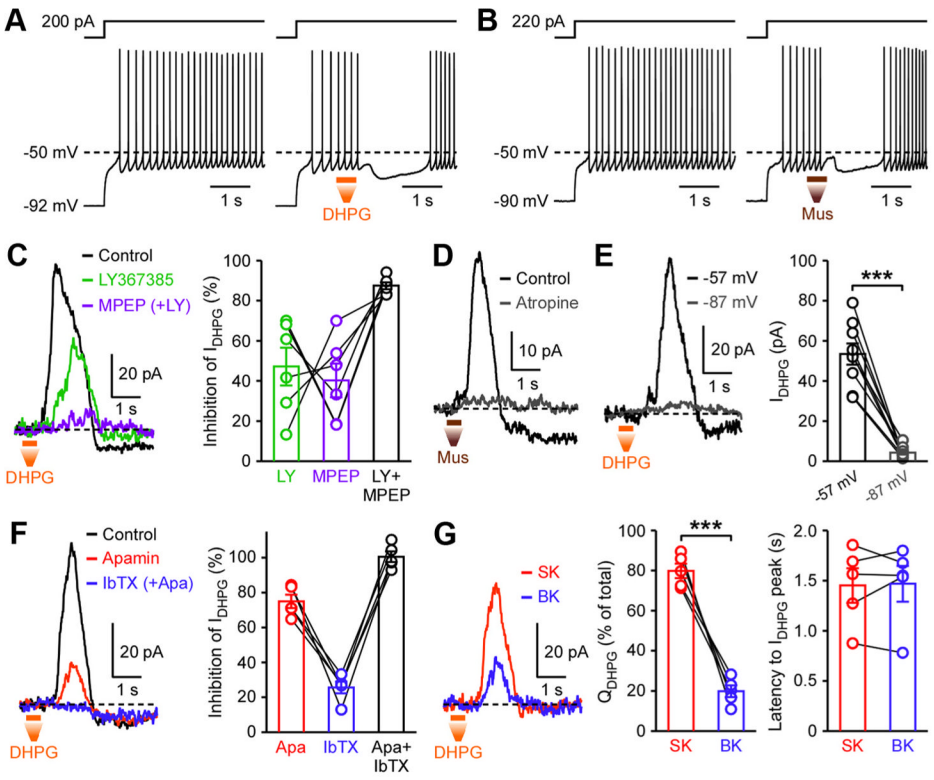

Figure 1.

Transient mGluR and mAChR activation produces pauses in SPN firing and activates SK and BK channels. ***A***, ***B***, Example traces depicting DHPG- and muscarine-induced pauses in SPN firing evoked by depolarizing current injections. Local pressure ejection (500 ms) of DHPG (100 μM) (***A***) or muscarine (100 μM) (***B***) was made at the time indicated. ***C***, Example traces and summary graph showing the effects of LY367385 (75 nM) and MPEP (50 nM) on I_{DHPG} (V_h = −57 mV). ***D***, Example traces illustrating the effect of atropine (2 μM) on muscarine-evoked currents. ***E***, Representative traces and summary graph showing that I_{DHPG} was suppressed by hyperpolarization to −87 mV ($t_{(8)}$ = 9.24, $p < 0.0001$; paired t test). ***F***, Example traces and summary graph depicting the effects of apamin (100 nM) and IbTX (100 nM) on I_{DHPG}. ***G***, Left, Traces of the apamin-sensitive SK-dependent component and the IbTX-sensitive BK-dependent component of I_{DHPG} shown in ***F***. These traces were obtained by subtracting traces before and after apamin/IbTX applications. Right, Summary graphs plotting the fraction of charge carried by SK- and BK-dependent components ($t_{(4)}$ = 9.68, $p < 0.001$; paired t test) and the latency to peak after the onset of DHPG pressure ejection. Error bars indicate SEM.

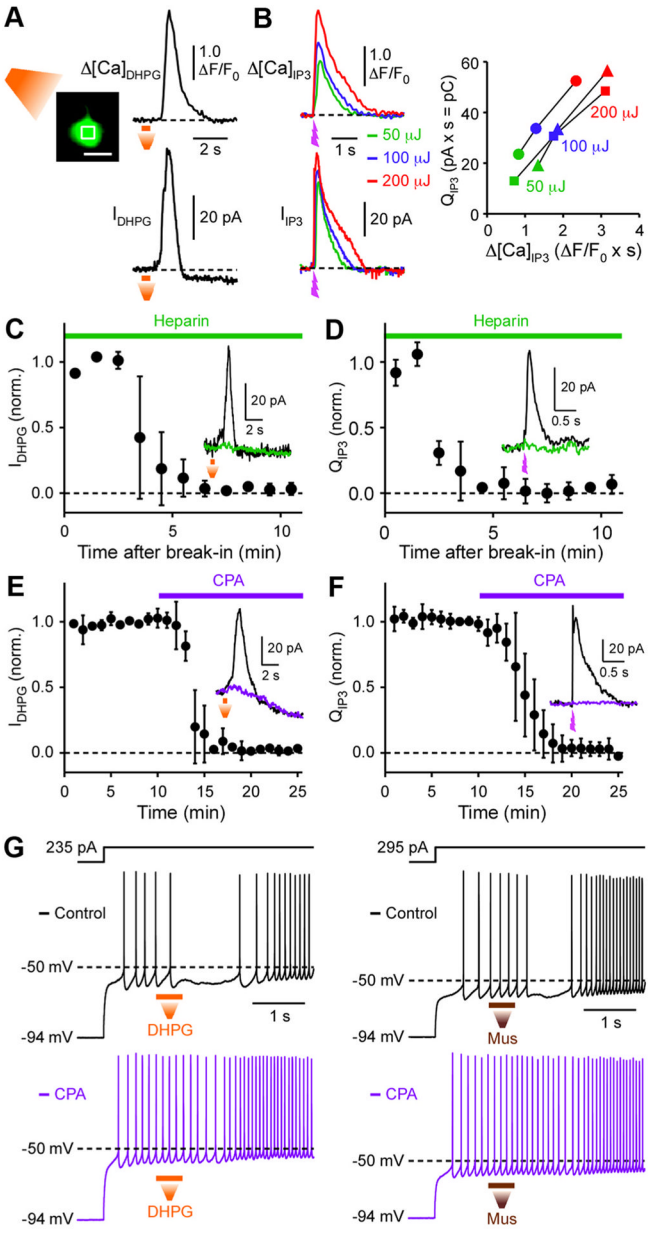

Figure 2.

IP_3R-dependent Ca^{2+} release from intracellular stores mediates mGluR/mAChR-induced SPN inhibition. ***A***, Representative experiment imaging DHPG-evoked Ca^{2+} transient. Fluorescence change, monitored at the ROI indicated on the left (scale bar: 10 μm), and an outward current evoked by pressure ejection of DHPG (100 μM; in a pipette placed ~60 μm from the recorded cell) are shown in an SPN loaded with Fluo-4FF (100 μM). Note that DHPG-evoked delayed inward current, which is independent of Ca^{2+} rise, outlasts the fluorescence change. ***B***, Example experiment monitoring Ca^{2+} transients and outward currents elicited by flash photolysis of caged IP_3 (400 μM) using three different UV flash intensities (50, 100, and 200 μJ). UV flashes were applied at the time indicated. Fluorescence changes were measured at the ROI placed in the soma as in ***A*** (cell image not shown). Right, The total charge transfer of I_{IP3} (termed Q_{IP3}) exhibited approximately linear relationship with the total fluorescence change (integrated over time) in three cells tested for

different UV intensities. Fluo-4FF (100 μM) was used to monitor $[Ca^{2+}]_i$ in these three cells. ***C–F***, Summary time graphs showing that cytosolic application of heparin (1 mg/ml) or bath application of CPA (20 μM) abolished outward currents elicited by DHPG (***C***, ***E***) and IP_3 (***D***, ***F***). Traces from a sample experiment are shown as an inset in each panel. ***G***, Example traces depicting that CPA suppressed the pauses in SPN firing produced by pressure ejection of DHPG (left) and muscarine (right). Note that DHPG and muscarine still caused delayed acceleration in firing after CPA treatment.

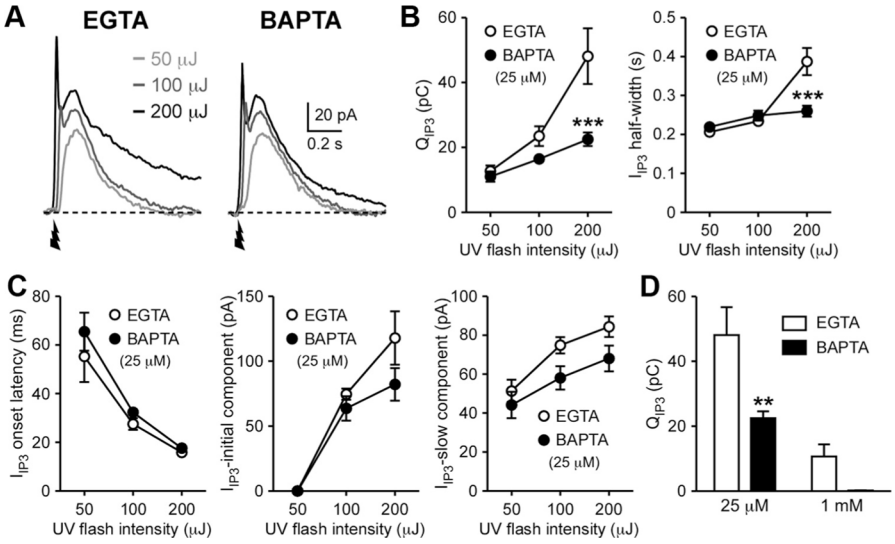

Figure 3.

IP_3 triggers BAPTA-sensitive localized Ca^{2+} signaling. ***A***, Representative traces of I_{IP3} using three different UV intensities (50, 100, and 200μJ) in cells filled with EGTA (25μM) and BAPTA (25μM). UV flashes were applied at the time indicated. ***B***, Summary plots showing the effects of BAPTA on Q_{IP3} (Ca^{2+} buffer type: $F_{(1,16)} = 6.22$, $p<0.05$; Ca^{2+} buffer concentration: $F_{(2,16)} = 36.2$, $p < 0.0001$; Ca^{2+} buffer type by concentration: $F_{(2,16)} = 10.1$, $p < 0.01$) and I_{IP3} half-width (Ca^{2+} buffer concentration: $F_{(2,16)} = 37.8$, $p < 0.0001$; Ca^{2+} buffer type by concentration: $F_{(2,16)} = 18.9$, $p < 0.0001$; mixed two-way ANOVA). ***$p < 0.001$ versus EGTA (Bonferroni's *post hoc* test). ***C***, Summary graphs plotting three parameters of I_{IP3} (onset latency, peak amplitude of the initial component, and peak amplitude of the late component) using three different UV flash intensities in cells filled with EGTA (25μM) or BAPTA (25μM). These parameters were not significantly affected by BAPTA.***D***, Summary bar graph showing the effects of two different concentrations (25μM and1mM) of EGTA and BAPTA on Q_{IP3} (200μJ UV intensity) (Ca^{2+} buffer type: $F_{(1,14)} = 11.7$, $p < 0.01$; Ca^{2+} buffer concentration: $F_{(1,14)} = 32.0$, $p < 0.0001$; two-way ANOVA). **$p < 0.01$ versus EGTA (Bonferroni's *post hoc* test). Error bars indicate SEM.

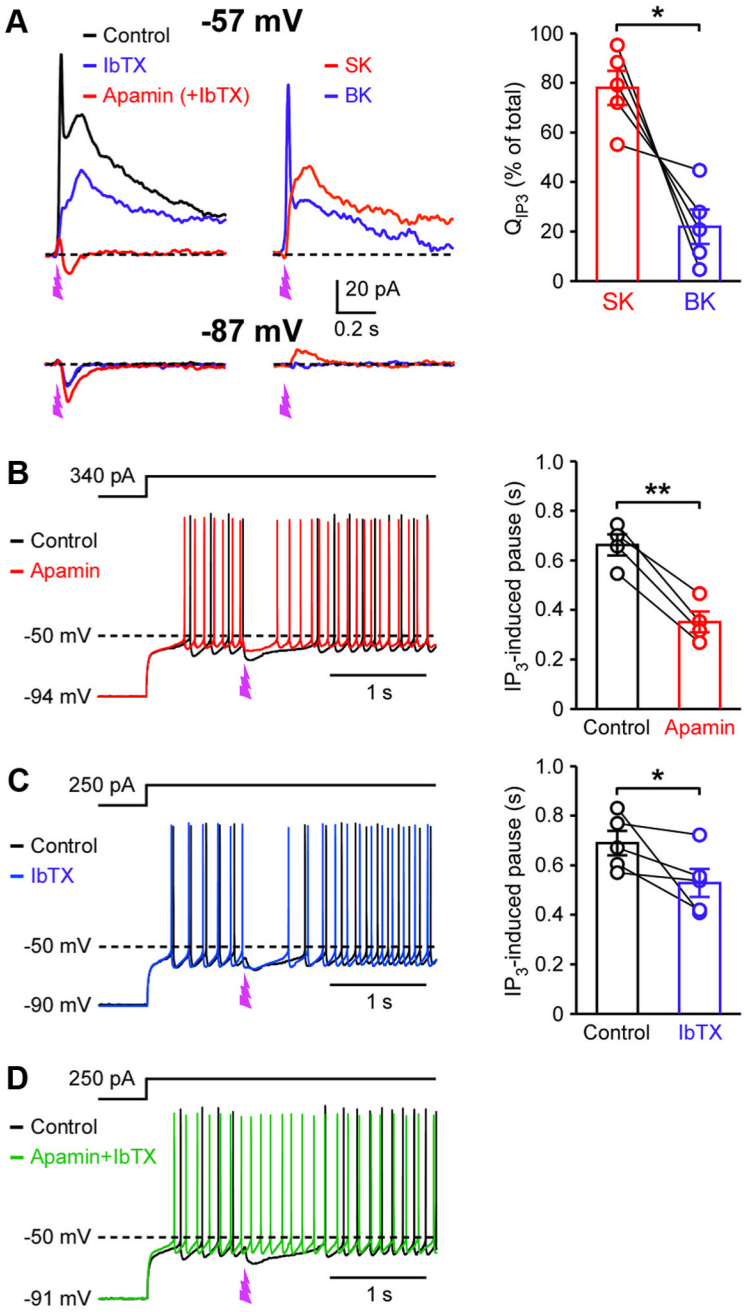

Figure 4.

IP_3-induced activation of SK and BK channels causes SPN inhibition. ***A***, Example traces showing the effects of apamin (100 nM) and IbTX (100 nM) on I_{IP3} (200 μJ UV intensity) measured at −57 and −87 mV. Traces of SK-and BK-dependent components were obtained by subtracting traces before and after apamin/IbTX applications. Note the absence of BK component at −87 mV, reflecting the voltage dependence of BK activation (Fakler and Adelman, 2008). Right, Summary graph plotting the fraction of charge carried by SK- and BK-dependent components at −57 mV ($t_{(4)} = 4.04$, $p < 0.05$; paired t test). ***B***, ***C***, Example traces depicting the effects of apamin (***B***) and IbTX (***C***) on IP_3-induced pause in SPN firing. The duration of IP_3-induced pause before and after application of apamin ($t_{(3)} = 9.06$; $p <$

0.01) or IbTX ($t_{(4)} = 2.27$, $p < 0.05$; paired *t* test) is plotted on the right. ***D***, Example traces showing that combined application of apamin and IbTX eliminated the IP_3-induced pause. Error bars indicate SEM.

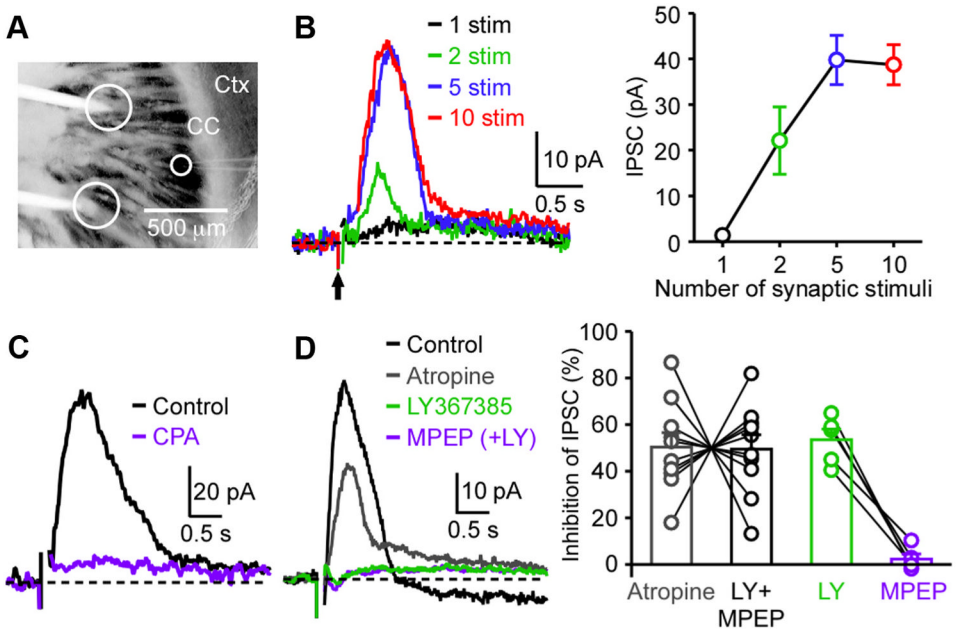

Figure 5.

Intrastriatal stimulation elicits Ca^{2+} store-dependent mGluR1/mAChR IPSCs. ***A***, Image of an oblique horizontal striatal slice depicting the placement of a bipolar stimulating electrode (tips inside large circles) with respect to the recorded cell (inside the small circle). Ctx, Cortex; CC, corpus callosum. ***B***, Example traces illustrating synaptic responses produced by trains of 1–10 intrastriatal stimuli (50 Hz). The arrow indicates the onset of stimulus trains. Stimulus artifacts are omitted from these traces for clarity. Right, Summary graph plotting the IPSC amplitude evoked by trains of 1–10 stimuli in four cells. ***C***, Representative traces showing the effect of CPA (20 μM). ***D***, Example traces and summary graph showing the effects of atropine (2 μM), LY367385 (75 nM), and MPEP (50 nM) on IPSCs. Percentage inhibition was calculated after removing the current insensitive to the combined application of these antagonists in each cell. Of 10 cells examined for all three antagonists, LY367385 and MPEP were applied together at the same time in 5 cells and sequentially in the remaining 5 cells. The order of drug application was varied in these experiments. Error bars indicate SEM.

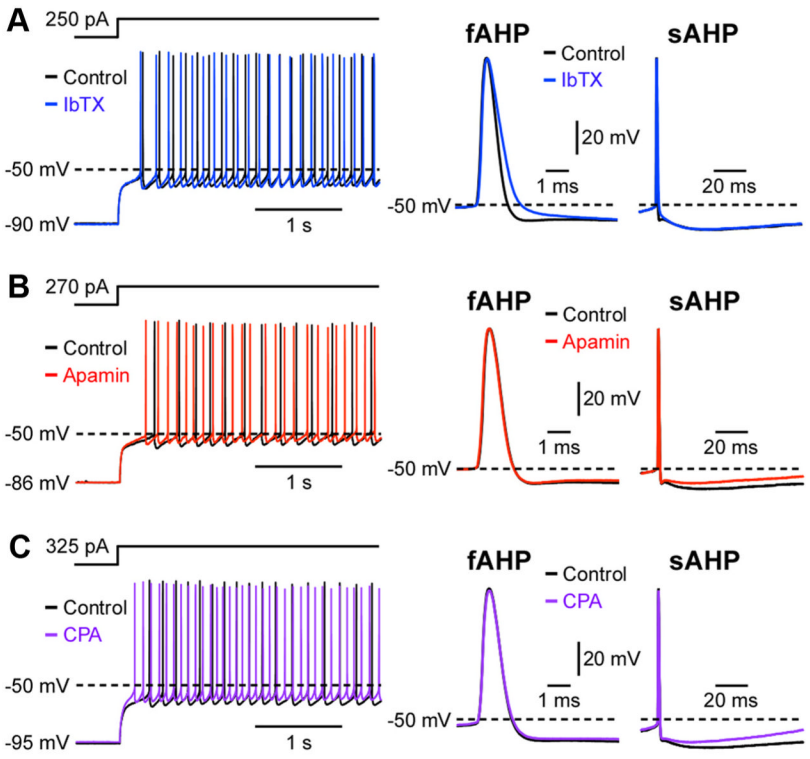

Figure 6.

Ca^{2+} release from intracellular stores regulates SK-dependent slow AHPs. Example traces showing the effects of IbTX (100 nM; ***A***), apamin (100 nM; ***B***), and CPA (20 μM; ***C***) on SPN firing. Right, First APs evoked by depolarizing current injections are shown on expanded timescales, with the AP onset aligned, to illustrate the effects of these drugs on the AP shape and two AHP components.

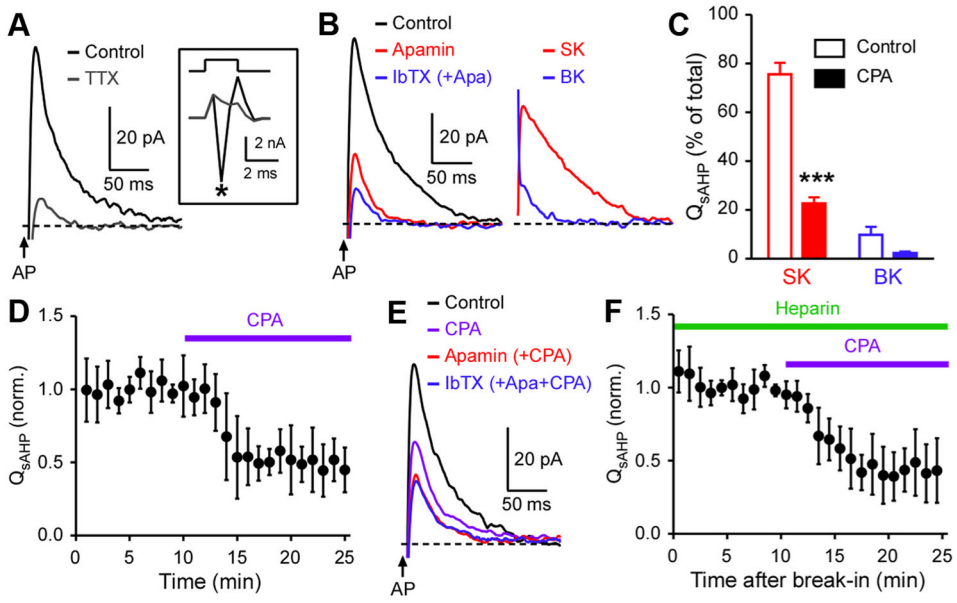

Figure 7.

Ca^{2+} store-dependent regulation of slow AHP currents is not dependent on IP_3Rs. ***A***, Example traces showing that TTX (1 mM) largely suppressed I_{sAHP}. Inset, Traces of currents during the 2 ms depolarization are shown on an expanded scale (2 Hz sampling frequency). Note that TTX abolished the inward action current (asterisk). ***B***, Example traces depicting the effects of apamin (100 nM) and IbTX (100 nM) on I_{sAHP} elicited by unclamped APs. Currents during unclamped APs (at the time indicated by the arrow) are omitted for clarity. Traces of SK- and BK-dependent components of I_{sAHP} are shown on the right. The small apamin/IbTX-insensitive component likely reflects activation of voltage-gated K^+ conductance. ***C***, Summary bar graph showing the fraction of Q_{sAHP} carried by SK- and BK-dependent components in control solution and after application of CPA (20 μM). Note that the data in CPA represent percentage of total Q_{sAHP} before CPA application in each cell [external solution (control vs CPA): $F_{(1,14)}$ =77.7, p <0.0001; current type (SK vs BK): $F_{(1,14)}$ =158, p <0.0001; external solution by current type: $F_{(1,14)}$ =43.9, p <0.0001; two-way ANOVA]. ***p <0.001 versus control solution (Bonferroni's *post hoc* test). ***D***, Summary time graph illustrating CPA-induced suppression of Q_{sAHP}. ***E***, Example traces of I_{sAHP} depicting the effects of CPA, apamin, and IbTX applied sequentially. ***F***, Summary time graph demonstrating that heparin failed to affect CPA-induced suppression of Q_{sAHP}. Error bars indicate SEM.

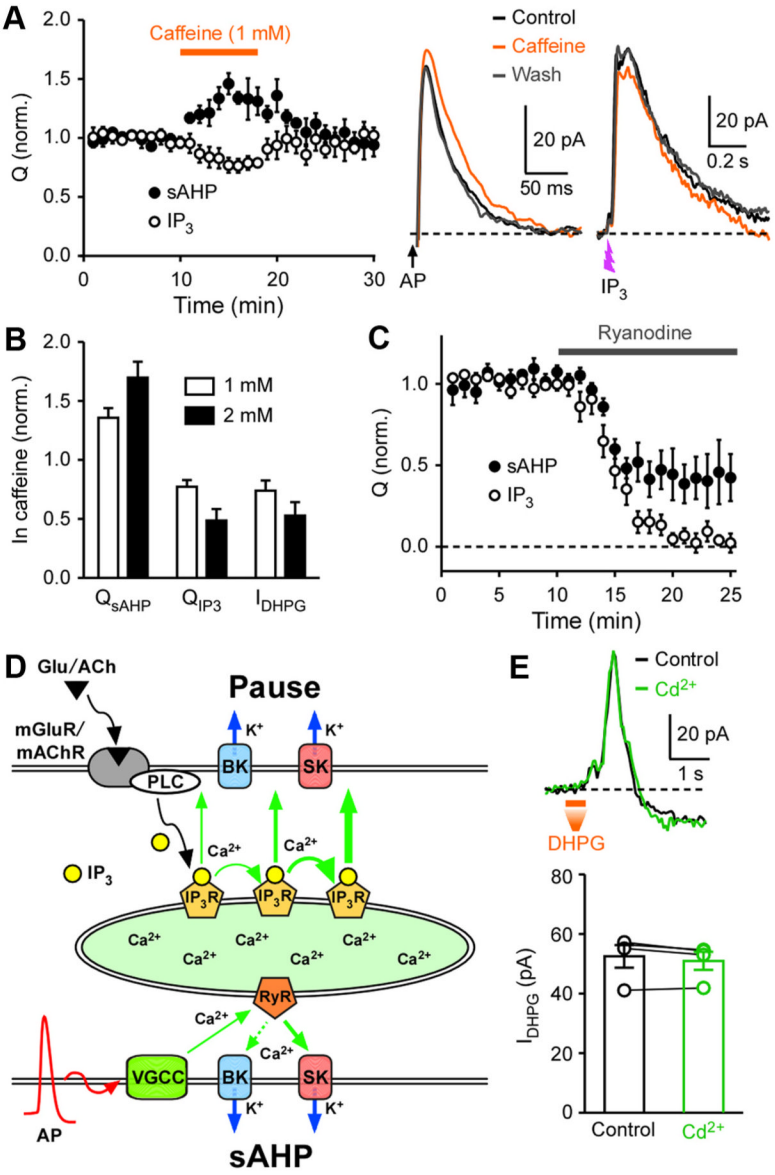

Figure 8.

Functional segregation of IP_3Rs and RyRs. ***A***, Summary time graph illustrating the effects of caffeine (1 mM) on Q_{sAHP} and Q_{IP3}. In these experiments, both I_{sAHP} and I_{IP3} were evoked once a minute (7 s apart) in each cell. Traces of I_{sAHP} and I_{IP3} from a sample experiment are shown on the right. ***B***, Summary bar graph showing the effects of caffeine (1 and 2 mM) on Q_{sAHP}, Q_{IP3}, and I_{DHPG}. ***C***, Summary time graph depicting ryanodine (20 μM)-induced depression of Q_{sAHP} and Q_{IP3}. ***D***, Schematic diagram illustrating the functional segregation two Ca^{2+} signaling pathways mediating Ca^{2+} store-dependent activation of SK and BK channels: (1) mGluR/mAChR →IP_3 →IP_3R pathway and (2) AP →VGCC →RyR pathway. This diagram does not include the direct coupling between VGCC-mediated Ca^{2+} influx and SK/BK channels (Fakler and Adelman, 2008). ***E***, Representative traces (top) and summary graph (bottom) showing that Cd^{2+} (100 μM) had no significant effect on I_{DHPG}. Error bars indicate SEM.

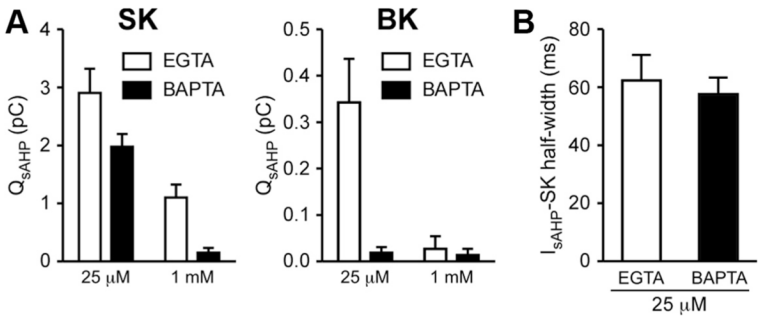

Figure 9.

BAPTA-sensitive localized Ca^{2+} signaling is involved in the generation of I_{sAHP}. ***A***, Summary bar graphs plotting SK-and BK-dependent components of Q_{sAHP} in cells filled with two different concentrations (25 μM and 1 mM) of EGTA or BAPTA (SK-dependent component: Ca^{2+} buffer type, $F_{(1,11)} = 7.90$, $p < 0.05$; Ca^{2+} buffer concentration, $F_{(1,11)} = 29.7$, $p < 0.001$; BK-dependent component: Ca^{2+} buffer type, $F_{(1,11)} = 6.08$, $p < 0.05$; Ca^{2+} buffer concentration, $F_{(1,11)} = 5.50$, $p < 0.05$, Ca^{2+} buffer type by concentration, $F_{(1,11)} = 5.15$, $p < 0.05$; two-way ANOVA). ***B***, Summary bar graph showing that BAPTA (25 μM) did not affect the half-width of the SK-dependent component of I_{sAHP} ($t_{(7)} = 0.43$, $p = 0.68$; unpaired *t* test). Error bars indicate SEM.

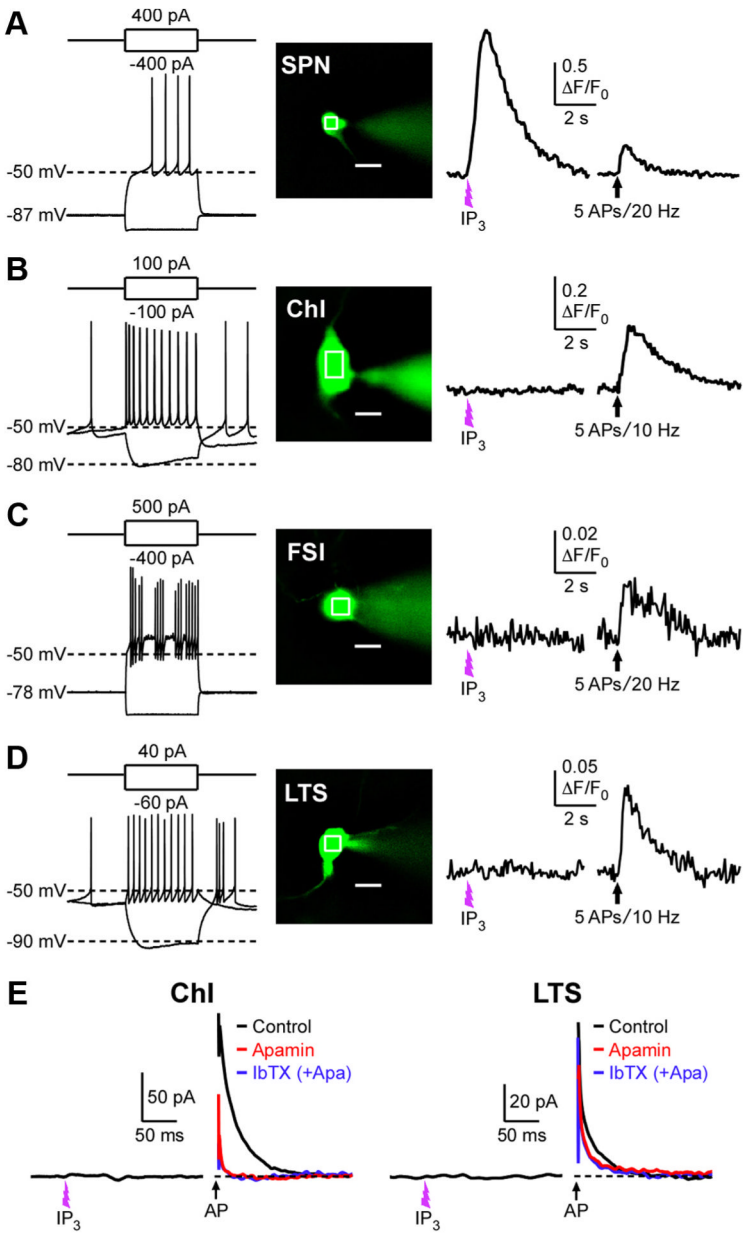

Figure 10.

Photolytic application of IP_3 produces Ca^{2+} transients only in SPNs among striatal neurons. ***A–D***, Representative traces of Ca^{2+} transients evoked by flash photolysis of caged IP_3 (400 μM) or trains of APs (5 APs at 10–20 Hz; train onset at the arrow) in an SPN (***A***), a ChI (***B***), an FSI (***C***), and an LTS interneuron (***D***). Neuron types were identified by characteristic responses to depolarizing and hyperpolarizing current injections (500 ms) (Kawaguchi, 1993). Fluorescence changes were monitored at the ROIs indicated in the images of cells filled with Fluo-4 (200 μM). Scale bar: 10 μm. Cells were voltage clamped at −57 mV in these experiments. ***E***, Example traces illustrating that photolytic application of IP_3 failed to elicit outward currents in a ChI and an LTS interneuron, although these neurons exhibited apamin-sensitive (i.e., SK-dependent) I_{sAHP} in response to unclamped APs (V_h = −57 mV). Error bars indicate SEM.

Table 1

Effects of IbTX, apamin, and CPA on electrophysiological properties of SPNs

	IbTX (*n* = 6)		Apamin (*n* = 6)		CPA (*n* = 8)		CPA in apamin (*n* = 4)	
	Control	**IbTX**	**Control**	**Apamin**	**Control**	**CPA**	**Apamin**	**CPA**
AP threshold (mV)	−46.6 ± 1.5	−46.8 ± 1.7	−47.6 ± 1.4	−48.2 ± 1.5	−47.3 ± 1.6	−47.7 ± 1.6	−48.2 ± 1.2	−49.5 ± 1.1
AP half-width (ms)	0.80 ± 0.02	1.05 ± 0.05 **	0.72 ± 0.02	0.73 ± 0.02	0.75 ± 0.02	0.76 ± 0.02	0.74 ± 0.02	0.75 ± 0.02
AP decay rate (ms)	0.38 ± 0.02	0.59 ± 0.03 **	0.33 ± 0.01	0.33 ± 0.01	0.35 ± 0.01	0.36 ± 0.01	0.34 ± 0.01	0.34 ± 0.00
Latency to first AP (ms)	567 ± 34	510 ± 23	560 ± 25	410 ± 21 **	551 ± 37	401 ± 51 **	437 ± 17	458 ± 22
Interspike interval (ms)	175 ± 6	174 ± 10	171 ± 8	101 ± 2 ***	159 ± 7	116 ± 11 **	104 ± 1	108 ± 5
fAHP amplitude (mV)	9.7 ± 0.6	4.0 ± 0.8 ***	10.2 ± 1.1	9.8 ± 1.1	11.5 ± 0.4	10.9 ± 0.4	11.1 ± 1.0	11.1 ± 1.1
sAHP amplitude (mV)	14.5 ± 0.5	14.2 ± 0.4	14.5 ± 0.4	11.3 ± 0.6 ***	14.4 ± 0.5	12.9 ± 0.4 **	12.0 ± 0.3	11.9 ± 0.4
RMP (mV)	−87.1 ± 1.6	−87.6 ± 1.3	−89.8 ± 1.1	−90.7 ± 1.3	−89.4 ± 1.7	−90.1 ± 2.0	−91.3 ± 0.9	−91.8 ± 1.0
Input resistance (MΩ)	61.0 ± 9.6	65.6 ± 11.1	53.2 ± 5.2	54.5 ± 5.4	56.1 ± 5.7	56.8 ± 5.5	53.3 ± 8.4	53.6 ± 8.5

* $p < 0.05$;

** $p < 0.01$;

*** $p < 0.001$ (paired *t* test).